IEEE Access
Multidisciplinary | Rapid Review | Open Access Journal

Received 8 November 2022, accepted 25 November 2022, date of publication 6 December 2022,
date of current version 12 December 2022.

Digital Object Identifier 10.1109/ACCESS.2022.3227050

RESEARCH ARTICLE

Biaxial FBG Vibration Sensor With a Single Edge Filter and Matching Demodulation

ABRAHAM PEREZ-ALONZO[1,2], FERNANDO VELÁZQUEZ-CARREÓN[1,2], AND GABRIEL EDUARDO SANDOVAL-ROMERO[2]

[1]Programa de Maestría y Doctorado en Ingeniería, Universidad Nacional Autónoma de México, Mexico City 04510, Mexico
[2]Instituto de Ciencias Aplicadas y Tecnología, Universidad Nacional Autónoma de México, Mexico City 04510, Mexico

Corresponding author: Abraham Perez-Alonzo (a.perez.iee.daia@gmail.com)

This work was supported by the Dirección General de Asuntos del Personal Académico—Universidad Nacional Autónoma de México (DGAPA-UNAM) under Project PAPIIT IT101019. The work of Abraham Perez-Alonzo was supported by the Consejo Nacional de Ciencia y Tecnología (CONACYT) through the master's and Ph.D. Engineering Program at the Universidad Nacional Autónoma de México.

ABSTRACT This work developed, simulated, and characterized a high sensitivity vibration sensor for low-frequency applications. The fiber Bragg grating (FBG) overlapping method was used to demodulate the wavelength shift of the sensing gratings, but only one FBG for each axis was utilized (unlike two FBGs in the common approach), along with another one acting as a filter for both axes and temperature compensator; this enhanced method could measure acceleration in two axes simultaneously, although only the X-axis had constant sensibility in the entire operating range. The difficulty in achieving constant sensitivity in both axes lies in the need to match three Bragg gratings, resulting in a set of gratings with similar Bragg wavelengths. The new results showed constant sensitivity in both accelerometer axes (0.735 and 0.684 $V \cdot m^{-1} \cdot s^2$ for the X- and Y-axis, respectively). The usable frequency and acceleration amplitude ranges were from 0.5 to 20 Hz and from 14×10^{-3} to 9 m/s^2, respectively, which both meet the requirements for detecting seismic-induced movements. Furthermore, the present results demonstrate that we can utilize a smaller number of gratings in accelerometer development compared to the common approach.

INDEX TERMS Biaxial accelerometer, FBG interrogation, vibration sensing, vibrometer.

I. INTRODUCTION

Buildings may be greatly affected by seismic movements, whose effect on them must thus be monitored. The response and health of buildings can be effectively assessed by measuring the spectral acceleration of their movement induced by ground motion [1], [2]. Optical sensors, compared to electronic ones, offer advantages such as electromagnetic interference immunity and high sensitivity that make them suitable for installation in all types of building, regardless of the electromagnetic noise level.

Several types of fiber Bragg grating (FBG)-based accelerometers have been developed in one, two, or three axes. For example, a uniaxial device includes a microstructure for measuring vibration and temperature simultaneously, within a 0.5–10 Hz range, and it uses filters and photodetectors to demodulate the FBG Bragg wavelength [3]. A two-dimensional (2D) vibration sensor [4] has been endowed with adjustable sensitivity to make it equal in both axes within a detection range of 0–180 Hz; however, no measurements under 20 Hz have been reported, and an interrogator was used to demodulate the FBG Bragg wavelength. A biaxial accelerometer using only 2 FBGs arranged on one axis and relying on axial and transverse forces has also been developed [5]. It has a resonant frequency of 34.42 Hz and needs an interrogator to demodulate its wavelength shift. Reference [6] presented a biaxial vibration sensor based on a multiaxis flexure hinge, with a measurement range of 5–170 Hz and the same sensitivity in the two axes. However, for the application at which our work aims, this frequency range is not sufficiently low and requires the use of an interrogator.

The associate editor coordinating the review of this manuscript and approving it for publication was Md. Selim Habib.

Besides the accelerometers listed above, the development of this kind of sensor has been focused mainly on uniaxial models [7]. Nonetheless, since vibration is a multidimensional vector signal, we developed a 2D sensor. As described above and reported in other studies [8], [9], [10], [11], [12], when researchers develop a new model, they use two FBGs for each axis when the edge filter demodulation method is utilized or a smaller number of FBGs but coupled with an interrogator. An interrogator with good precision and scanning speed has a high cost that is affordable for distributed sensing but not for applications in independent sensors. In our previous work [13], we proposed a biaxial vibration sensor that uses only one FBG for each axis and does not need an interrogator, but we could not attain constant sensitivity in both axes in its measurement range.

In addition to the experimental work, this work also includes sensor simulation and in-depth theoretical analysis of the physical structure. Additionally, we changed the characteristics of its sensing FBGs, specifically the central Bragg wavelength, to better approximate the optimal operation point where the FBG response to deformation is linear. With this modification, we achieved a better sensing performance with almost constant sensitivity in both axes within the target range, which is intended for measuring the building's response to seismic ground motions; our previous work was unable to achieve this performance.

The proposed application for this sensor in seismically active areas is critical, and it is unique because each monitoring structure, such as buildings, tunnels, or bridges, has specific frequency and amplitude measurement requirements. This sensor is an additional option for measurement vibration applications.

First, the working principle and theoretical model of the accelerometer is discussed in this study. Then, a finite element analysis (FEA) simulation of the sensor's natural frequency, conducted to verify the theoretical results, is reported. Finally, the experimental results for the sensitivity, frequency response, and natural frequency of the sensor are presented.

II. WORKING PRINCIPLE

A. FBG

An FBG is essentially a temperature and strain sensor. Its Bragg wavelength (λ_B) is determined by the effective refractive index of the fiber core (n_{eff}) and the grating period (Λ) as follows:

$$\lambda_B = 2n_{eff}\,\Lambda. \tag{1}$$

A change in temperature and axial strain will cause a wavelength shift ($\Delta\lambda_B$) in the FBG:

$$\frac{\Delta\lambda_B}{\lambda_B} = (\alpha + \eta)\,\Delta T + (1 - \rho_e)\,\Delta\varepsilon, \tag{2}$$

where α is the thermal expansion coefficient of FBG, η is the thermo-optic coefficient of FBG, ΔT is the temperature variation, ρ_e is the fiber optic photoelastic coefficient, and $\Delta\varepsilon$ is the axial strain.

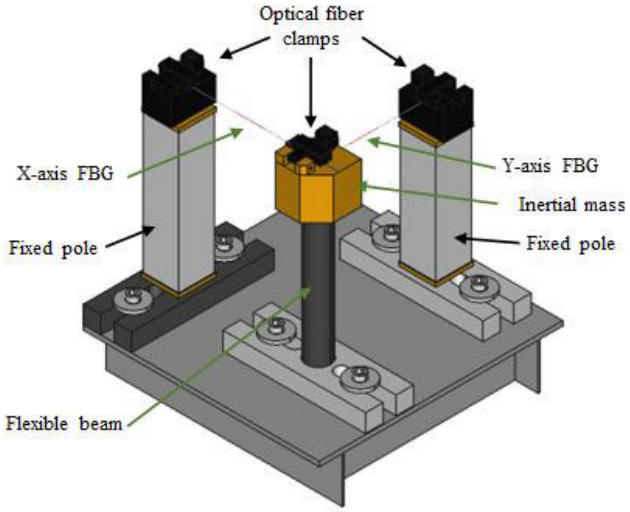

FIGURE 1. Structure of two-dimensional fiber Bragg grating accelerometer.

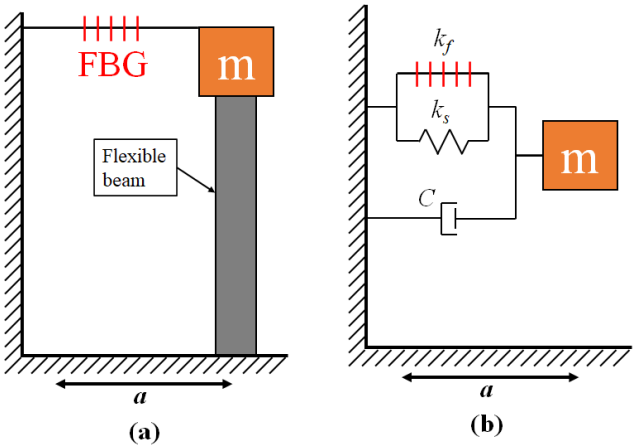

FIGURE 2. (a) Schematic structure of a one-dimensional second-order system and (b) its equivalent model.

When an appropriate interface is designed, other physical quantities can be measured with respect to the temperature or strain change in the FBG. The vibration applied to the whole accelerometer results in a strain change in the FBGs.

The accelerometer proposed has a reference FBG that acts as an edge filter in the optical demodulation scheme, which is not affected by the acceleration. Moreover, this FBG allows us to cancel the temperature effects in the output signal of the sensor, simplifying (2) as follows:

$$\frac{\Delta\lambda_B}{\lambda_B} = (1 - \rho_e)\,\Delta\varepsilon. \tag{3}$$

B. STRUCTURE AND THEORETICAL MODEL

Fig. 1 displays the structure of the proposed sensor, which consists of a flexible cylindrical beam, an inertial mass (m), one FBG for each sensing axis, and fixed parts with respect to the sensor movement. The fibers are fixed to optical fiber clamps by pressure.

To analyze this biaxial sensor, we consider it as two independent one-dimensional systems (Fig. 2). According to Newton's laws of motion, a one-dimensional system is equivalent to a second-order vibration system. k_s is the bending stiffness of the flexible beam, and the FBG is represented as a spring with a tension stiffness coefficient of k_f.

From the mechanics of materials, k_f can be expressed as

$$k_f = \frac{E_f A_f}{L_f}, \tag{4}$$

where E_f and A_f are the Young's modulus and cross-section area of the optical fiber, respectively, and L_f is the length of the fiber between the fixed points.

The k_s values can be obtained as

$$k_s = \frac{3E_s I_s}{L_s^3}, \tag{5}$$

where E_s and L_s are the Young's modulus and length of the flexible beam, respectively, and I_s is its second moment of inertia, which is equal in all directions and given by $I_s = (\pi/4)r^4$, where r is its radius.

When the excitation frequency is much lower than the natural angular frequency (ω_0), the sensitivity (S) and first resonant frequency (f_0) for the one-dimensional system are expressed as follows [9]:

$$S = \frac{m\,(1-\rho_e)\,\lambda_B}{k_s L_f + E_f A_f} \tag{6}$$

and

$$f_0 = \frac{1}{2\pi}\sqrt{\frac{k_s L_f + E_f A_f}{m L_s}}, \tag{7}$$

Equations (6) and (7) are used to calculate the S and f_0 for each axis of the accelerometer.

C. WAVELENGTH INTERROGATION SCHEME

Fig. 3 illustrates the interrogation scheme of the sensor, which can be divided into an upper and a lower branch corresponding to the X- and Y-axis, respectively. This optical scheme allows us to demodulate the Bragg wavelength by overlapping each sensing FBG with the same reference FBG (FBG_{REF}). Unlike the two FBGs commonly used for each axis, which would result in four FBGs for a biaxial accelerometer, we use only three FBGs without losing the ability to compensate for the induced Bragg wavelength shift caused by temperature changes. FBG_{REF} is subject to acceleration but is attached at both ends with fixed fiber clamps; thus, it is only affected by temperature changes. A detailed explanation of the principle of this method is provided in [14], [15] and for this specific approach in [13].

III. FEA SIMULATION

For the sensor simulation, the free software FreeCAD was used to model the structure, build the assembly, and perform the frequency analysis. Then, the simulation results were visualized with Paraview. The simulation included the flexible beam where the inertial mass component is on, the X- and Y-axis optical fibers, and the inertial mass.

The inertial mass was made of polylactic acid. The flexible beam was made of polyamide 6/6, which is a long-lasting material [16]. All the other parts (i.e., sensor base, fixed poles, and optical fiber clamps) were made of aluminum, except for the clamp fixing one end of each fiber and the inertial mass (see Fig. 1).

The accelerometer parameters used in the FEA for the frequency analysis are summarized in Table 1.

Fig. 4 displays the finite element mesh of the sensor, which was obtained using second-order tetrahedral elements for better accuracy in the curved shapes, with fixed constraints applied to the base. The element sizes were divided into regions with smaller elements in curved shapes, especially for the optical fibers, to achieve better accuracy, whereas bigger element sizes were organized in plane shapes to optimize the computational resources. The maximum element size was 0.1, 2, 4, and 15 mm for, respectively, the optical fibers, the flexible beam, the optical fiber clamps, and the base and

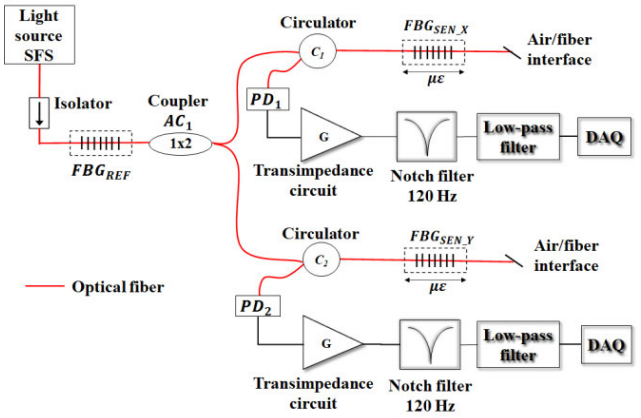

FIGURE 3. Optical scheme of the biaxial fiber Bragg grating accelerometer (SFS: superluminescent fiber source; PD_1 and PD_2: photodetectors; DAQ: data acquisition system).

TABLE 1. Sensor parameters.

Symbol	Parameter	Value
E_s	Young's modulus of the cylindrical beam	2.93 GPa
μ	Poisson's ratio of the cylindrical beam	0.39
d_s	Diameter of the cylindrical beam	13.0 mm
L_s	Length of the cylindrical beam	91.1 mm
E_{Al}	Young's modulus of the Al parts	70 GPa
E_f	Yung's modulus of the fiber with acrylate coating [17]	16.56 GPa
d_f	Diameter of the fiber with an acrylate coating	0.25 mm
m	Inertial mass	22.88 g
L_x	Distance between the fixed points of the X-axis	55.9 mm
L_y	Distance between the fixed points of the Y-axis	56.2 mm

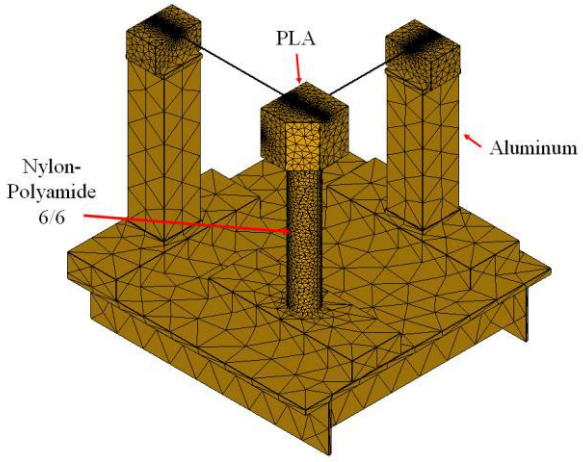

FIGURE 4. Finite element mesh of the sensor (PLA: polylactic acid).

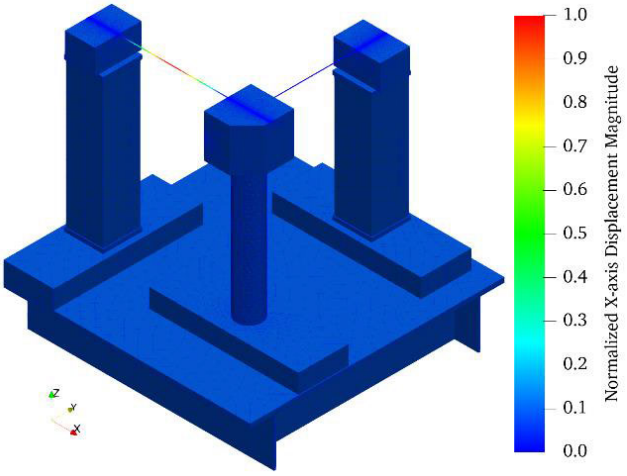

FIGURE 5. Three-dimensional view of the normalized displacement for the first resonant frequency of the accelerometer X-axis.

fixed poles. As a result, the first-order natural frequency was 171.6 Hz on the X-axis and 172.6 Hz on the Y-axis; the normalized displacements are illustrated in Fig. 5 and Fig. 6. In both cases, the point with maximum displacement was at the center of the optical fiber.

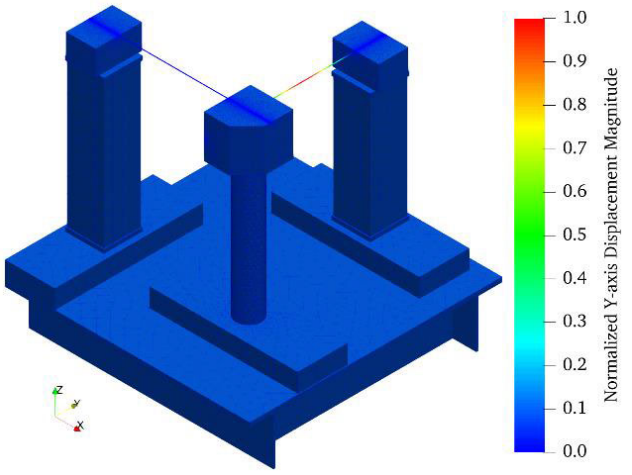

FIGURE 6. Three-dimensional view of the normalized displacement for the first resonant frequency of the accelerometer Y-axis.

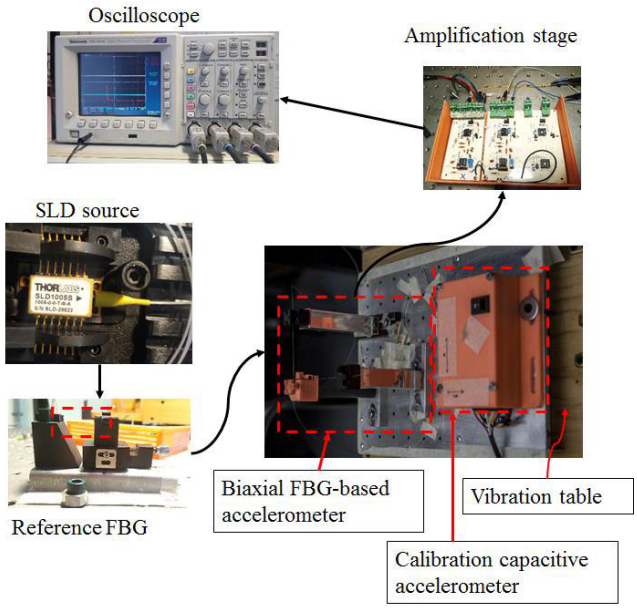

FIGURE 7. Vibration test system (SLD: superluminescent diode; FBG: fiber Bragg grating).

IV. EXPERIMENTAL SETUP

Fig. 7. shows the vibration test system. A superluminescent diode (SLD) (SLD1005S, Thorlabs) with a 50 nm bandwidth, a near-Gaussian spectral profile, and low ripple, together with a current and temperature controller (LDC3744B, ILX Lightwave) provided light with 1 mW of constant power at 1550-nm central wavelength. The light passed through the reference FBG, as shown in Fig. 3, and reached the optical sensor. The proposed biaxial FBG vibration sensor and an encapsulated arrange of three uniaxial capacitive accelerometers (MMA2260D and MMA1260D) arranged orthogonally were fixed in a vibration table. The vibration table is driven by a universal motor, with a set of pulleys providing a vibration range of 0.1–50 Hz in an almost sinusoidal waveform. The arrangement of capacitive accelerometers was used as a reference to know the input excitation acceleration to the optic sensor. Then, the output light carrying information on the vibration as its intensity changes reached a photodetector (PD-A-25, oeMarket) with a bandwidth of 2.5 GHz and a responsivity of 0.9 A/W at 1550 nm; the amplification stage included a transimpedance circuit for the photodetector and signal conditioning to visualize the information as a voltage through an oscilloscope.

Three FBGs with acrylate coating on the SMF-28e fibers and similar Bragg wavelengths (oeMarket.com) were used in this work. The length, reflectivity, and bandwidth of each FBG were 5 mm, >95%, and 0.2 nm, respectively. The initial central wavelengths at 21.0°C of the reference FBG,

X-axis FBG, and Y-axis FBG were 1549.449, 1549.470, and 1549.439 nm, respectively; they were measured by an optical spectrum analyzer (Fiberer-OSA-M-(1525-1565), Fiberer) with an operating wavelength range of 1525–1565 nm, 2-pm wavelength resolution, an operating optic power range of −75 to +5 dBm, and wavelength repeatability of ±5 pm. When the FBGs were mounted, a prestress was applied to them and their central wavelengths were left as close as possible. After the FBGs were fixed, the final wavelengths were 1549.637 and 1549.640 pm for the X- and Y-axis, respectively. Finally, the Bragg wavelength of the reference FBG was tuned using a translation stage to leave it in the central operation point [13].

V. RESULTS AND DISCUSSION

A. NATURAL FREQUENCY

The natural frequency of the sensor is an important parameter that affects its sensitivity and working frequency range. An impulse signal contains all frequencies; hence, an input impulse signal was applied to the vibration table to determine the natural frequency of our accelerometer. The impulse response observed in the oscilloscope was recorded, obtaining its frequency spectrum. The time domain response and corresponding frequency spectrum for the accelerometer X- and Y-axis are shown in Fig. 8 and Fig. 9, respectively.

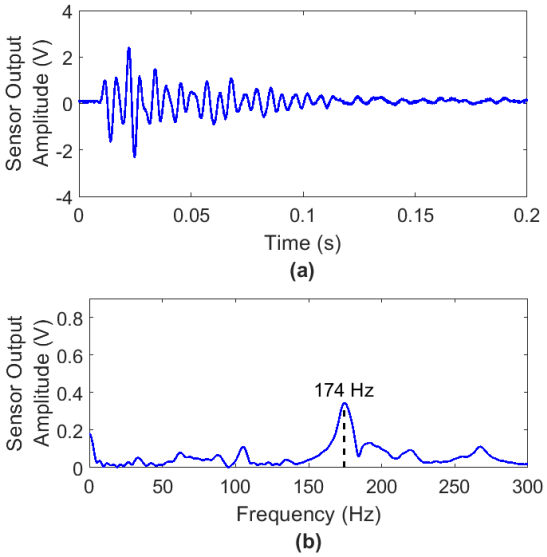

FIGURE 8. (a) Impulse response of the accelerometer X-axis in the time domain and (b) corresponding frequency spectrum.

The X and Y axes have been chosen in a horizontal plane because buildings preferentially move in a horizontal XY plane in a seismic event. The X and Y axes are orthogonally arranged.

The experimental resonant frequency of the accelerometer was about 174 Hz and 182 Hz for the X- and Y-axis, respectively. We calculated the theoretical natural frequency of the accelerometer by substituting, in (7), L_f with L_x and L_y (i.e., for the X- and Y-axis), whose values were 184.7 and 184.5 Hz, respectively.

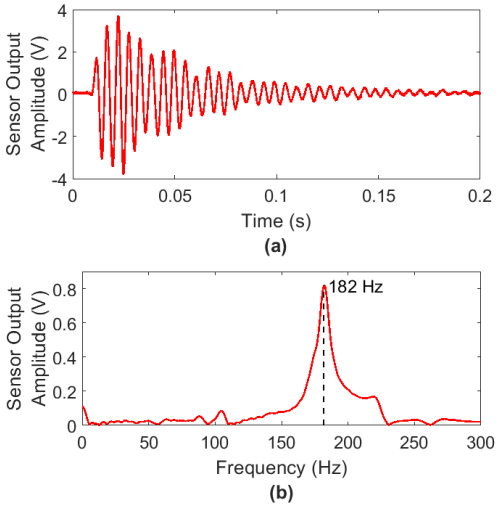

FIGURE 9. (a) Impulse response of the accelerometer Y-axis in the time domain and (b) corresponding frequency spectrum.

TABLE 2. Theoretical, Simulated, and experimental natural frequency of the accelerometer.

Natural frequency	X-axis	Y-axis
Theoretical	184.7 Hz	184.5 Hz
Simulated	171.6 Hz	172.6 Hz
Experimental	174 Hz	182 Hz

Table 2 shows the theoretical, simulated, and experimental natural frequencies of our accelerometer for the X- and Y-axis, with relatively small discrepancies, indicating that all results are valid. These small differences may be due to errors in some parameters, such as the stiffness coefficients of the optical fiber and flexible beam as well as the inertial mass density.

Since the frequency range of interest in the current study is 0.5–20 Hz, the natural frequency of our sensor on both axes is more than twice the maximum frequency of interest and, thus, could provide a reasonably uniform sensitivity curve in the lower-frequency region.

B. FREQUENCY RESPONSE AND SENSITIVITY

The biaxial FBG-based sensor was characterized through an amplitude–frequency scanning experiment in the 0.5–50 Hz range, whereas the input acceleration amplitude varied from 0.02 to 8.5 m/s^2.

The output amplitudes of the capacitive and optical sensors were recorded and processed on a computer to determine their sensitivity with respect to the experimental frequency range.

The theoretical sensitivity of the optical accelerometer was derived from (6) using $\rho_e = 0.22$ and $\lambda_B = 1.55$ μm, giving 16×10^{-12} s^2. This is a reasonable sensitivity value since we used a reference FBG as an edge filter matched with the sensing FBGs, all the FBGs had a bandwidth of 0.2 nm, and hence the Bragg wavelength change where it is proportional to the photodetector input power was 150 pm [13]. Therefore,

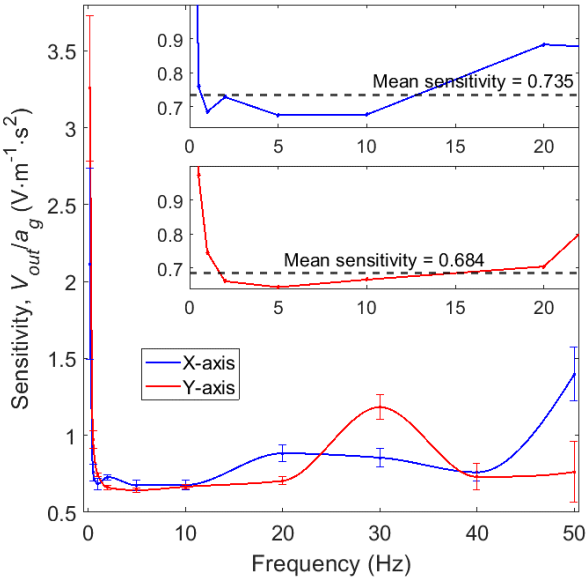

FIGURE 10. Sensitivity of the optical sensor as a function of the frequency, along with an amplification of the X- and Y-axis response in the range of interest (insets).

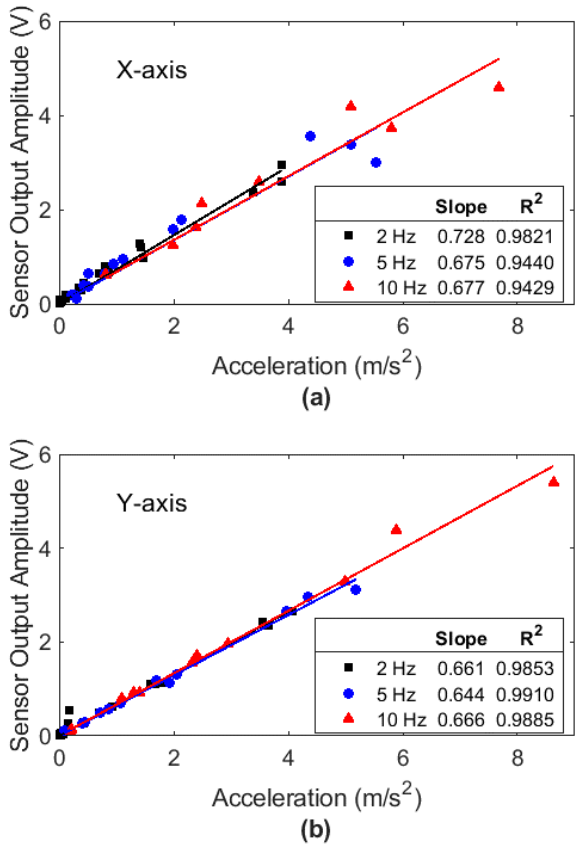

FIGURE 11. Amplitude of the sensor output versus applied acceleration at different excitation signals.

our sensor could measure in an acceleration amplitude range that was 9 m/s^2 wide.

Instead of the Bragg wavelength changes of the sensing FBGs, we measured the sensor output voltage (V_{out}), which

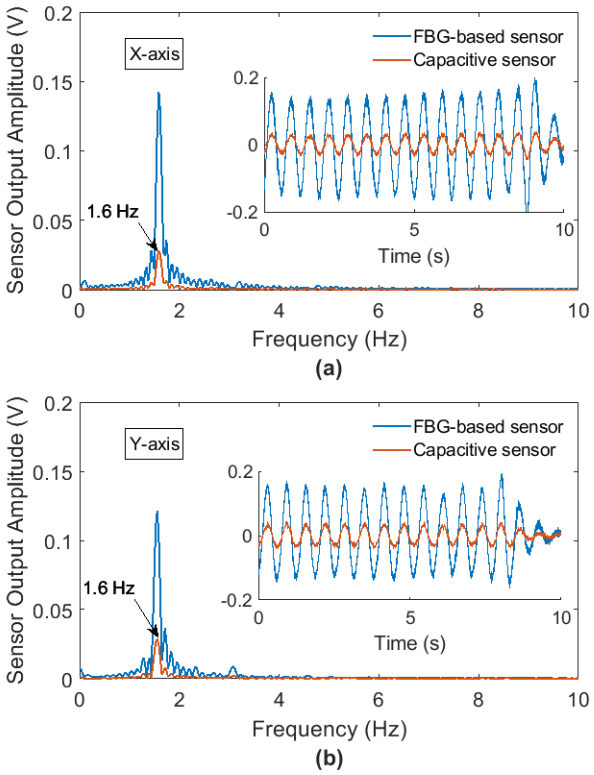

FIGURE 12. Output amplitude in the time and frequency domains of the fiber Bragg grating-based sensor and capacitive sensor (reference) for an input peak acceleration of 0.25 m/s^2 at 1.6 Hz: (a) X-axis and (b) Y-axis.

is proportional to such changes, and the acceleration input (a_g). Fig. 10 plots the sensitivity of the optical sensor against the frequency and also shows an amplification of the frequency range of interest (0.5–20 Hz), where the sensitivity was almost constant with an average value of 0.735 and 0.684 V·m^{-1} · s^2 for the X- and Y-axis, respectively.

C. LINEARITY OF THE BIAXIAL FBG SENSOR

We analyzed the linear response of the accelerometer. Sensor amplitude output is shown in the Fig. 11 as a function of the applied acceleration at different excitation signals (2, 5, and 10 Hz), along with the fitter curves. These experimental results indicate that our FBG accelerometer has good linearity with an R^2 value between 0.985 and 0.991, R^2 is the coefficient of determination. The specific sensitivity at 2, 5, and 10 Hz was, respectively, 0.728, 0.675, and 0.677 V·m^{-1}·s^2 for the X-axis and 0.661, 0.644, and 0.666 V·m^{-1}·s^2 for the Y-axis.

D. COMPARISON OF FBG ACCELEROMETER RESPONSE WITH REFERENCE ACCELEROMETER

Fig. 12 compares the output signals of the capacitive and optical sensors of an arbitrary input vibration of 1.6 Hz; the fast Fourier transform was applied to the recorded signal. The detected frequency was the same in the two accelerometers, demonstrating the good response of the optical sensor. The output waveform was also the same. The amplitude of the

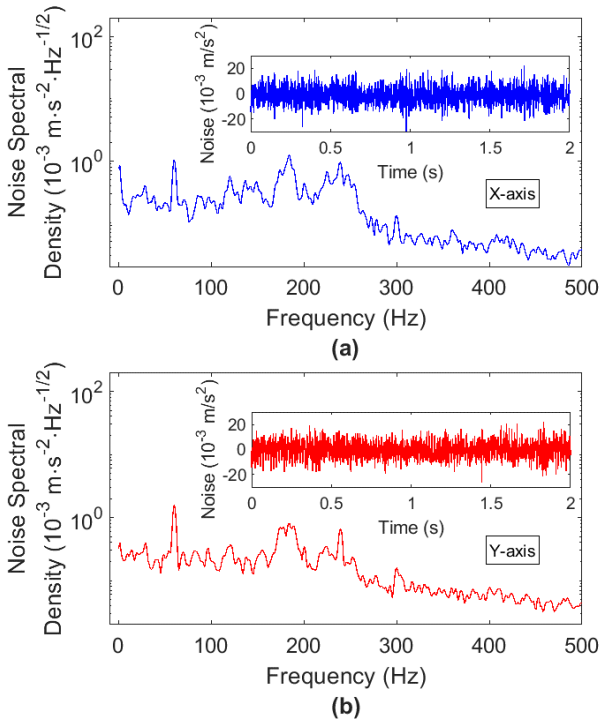

FIGURE 13. Noise in the time domain of the fiber Bragg grating accelerometer (inset) and equivalent acceleration spectral density: (a) X-axis and (b) Y-axis.

output signals, instead, differed due to the different sensitivity coefficients of the accelerometers.

E. NOISE ANALYSIS

Fig. 13 shows the noise and its equivalent spectral density between 0 and 500 Hz. The proposed sensor exhibited low noise dominated by the 60 Hz power line: about 1×10^{-3} m·s^{-2}·Hz$^{-1/2}$ on the X-axis and 1.6×10^{-3} m·s^{-2}·Hz$^{-1/2}$ on the Y-axis.

The root-mean-square value of the noise was 5.0 and 4.1 mV for the X- and Y-axis, respectively. Given the accelerometer mean sensitivity and a signal-to-noise ratio of 2, the minimum detectable acceleration was 14×10^{-3} m/s^2 for the X-axis and 12×10^{-3} m/s^2 for the Y-axis.

F. DYNAMIC RANGE

The dynamic range (DR) is an important parameter that reflects the ratio between the strongest and weakest detection signals. In the case of our accelerometer, it expresses the relationship between maximum (a_{max}) and minimum acceleration (a_{min}):

$$DR = 20log\left(\frac{a_{max}}{a_{min}}\right). \tag{8}$$

For the FBG accelerometer, a_{max} was limited to 9 m/s^2 by the linear range of the wavelength shift of the sensing FBGs in the overlapping interrogation scheme, whereas a_{min} was limited by the noise. According to (8), DR was 56 and 57 dB for the X- and Y-axis, respectively, in the target range of frequency.

VI. CONCLUSION

We presented a vibration sensor that uses an enhanced FBG overlapping interrogation method, which allows us to utilize a smaller number of FBGs compared with the traditional FBG overlapping method. We also described its working principle and reported simulation and experimental results, which agreed with each other. This sensor has almost constant sensitivity, with a mean value of 0.735 and 0.684 V·m^{-1}·s^2 in the X- and Y-axis, respectively, in the 0.5–20 Hz range. The frequency range of this accelerometer makes it suitable for seismic applications and in places with electromagnetic noise to measure, for instance, the response of a building to ground motion. Its minimum acceleration detection is about 14×10^{-3} m/s^2, which corresponds to a weak shaking felt only by a few persons at rest, especially on the upper floors of buildings.

Since the proposed sensor has a high degree of sensitivity, it can be used in other applications, such as inertial navigation systems. This sensor can be used to measure vibration in rotating electrical machines in their current configuration by adjusting parameters such as inertial mass and the material of the flexible beam, i.e., the modulus of elasticity of the material.

Furthermore, this sensor does not need an interrogator for individual measurement points. The use of sensing FBGs with similar central wavelength (a difference below 21 pm before prestress, which was even reduced to 3 pm after prestress) allows their tuning. The central wavelengths of the sensing FBGs in the proposed interrogation scheme must be as close as possible to achieve the best performance in both axes.

REFERENCES

[1] J. W. Baker and C. A. Cornell, "Which spectral acceleration are you using?" *Earthq. Spectra*, vol. 22, no. 2, pp. 293–312, May 2006.
[2] A. Elenas, "Correlation between seismic acceleration parameters and overall structural damage indices of buildings," *Soil Dyn. Earthq. Eng.*, vol. 20, nos. 1–4, pp. 93–100, Oct. 2000.
[3] Q. Zhang, T. Zhu, J. Zhang, and K. S. Chiang, "Micro-fiber-based FBG sensor for simultaneous measurement of vibration and temperature," *IEEE Photon. Technol. Lett.*, vol. 25, no. 18, pp. 1751–1753, Sep. 15, 2013.
[4] J. Wang, L. Wei, R. Li, Q. Liu, L. Yu, T. Li, and Y. Tan, "An FBG-based 2-D vibration sensor with adjustable sensitivity," *IEEE Sensors J.*, vol. 17, no. 15, pp. 4716–4724, Aug. 2017.
[5] K. Li, T. H. T. Chan, M. H. Yau, D. P. Thambiratnam, and H. Y. Tam, "Biaxial fiber Bragg grating accelerometer using axial and transverse forces," *IEEE Photon. Technol. Lett.*, vol. 26, no. 15, pp. 1549–1552, Aug. 1, 2014.
[6] L. Wei, L. Yu, J. Wang, D. Jiang, Q. Liu, and Z. Liu, "An FBG-sensing two-dimensional vibration sensor based on multi-axis flexure hinge," *IEEE Sensors J.*, vol. 19, no. 10, pp. 3698–3710, May 15, 2019.
[7] T. Li, J. Guo, Y. Tan, and Z. Zhou, "Recent advances and tendency in fiber Bragg grating-based vibration sensor: A review," *IEEE Sensors J.* vol. 20, no. 20, pp. 12074–12087, Jun. 2020.
[8] T. Guo, T. Zhang, Y. Li, and X. Qiao, "Highly sensitive FBG seismometer with a 3D-printed hexagonal configuration," *J. Lightw. Technol.*, vol. 38, no. 16, pp. 4588–4595, Aug. 15, 2020.

[9] Q. Liu, W. Liu, C. Wang, R. Zhang, W. Fan, D. Yu, and X. Qiao, "High figure of merit and low cross sensitivity fiber Bragg grating accelerometer based on double grid-diaphragms," *IEEE Sensors J.*, vol. 21, no. 24, pp. 27503–27509, Nov. 2021.
[10] H. Song, E. Song, W. Peng, B. Wang, Y. Liu, G. Zhao, and M. Liu, "Miniature structure optimization of small-diameter FBG-based one-dimensional optical fiber vibration sensor," *IEEE Sensors J.*, vol. 21, no. 23, pp. 26763–26771, Dec. 2021.
[11] X. Zhao, Z. Jia, W. Fan, W. Liu, H. Gao, K. Yang, and D. Yu, "A fiber Bragg grating acceleration sensor with temperature compensation," *Optik*, vol. 241, Sep. 2021, Art. no. 166993.
[12] J. Li, B. Shen, D. Zhao, W. Zhang, and B. Sun, "A high-sensitivity FBG accelerometer based on a bearing," *J. Lightw. Technol.*, vol. 40, no. 1, pp. 228–236, Jan. 1, 2022.
[13] A. Perez-Alonzo and G. E. Sandoval-Romero, "Accelerometer prototype based on enhanced fiber Bragg grating overlapping interrogation method," *Optik*, vol. 242, Sep. 2021, Art. no. 167027.
[14] A. B. L. Ribeiro, L. A. Ferreira, J. L. Santos, and D. A. Jackson, "Analysis of the reflective-matched fiber Bragg grating sensing interrogation scheme," *Appl. Opt.*, vol. 36, no. 4, pp. 934–939, Feb. 1997.
[15] M. A. Casas-Ramos and G. E. Sandoval-Romero, "Strain detection and measurement using a matched fibre Bragg grating," *J. Electromagn. Waves Appl.*, vol. 32, no. 12, pp. 1519–1526, Aug. 2018.
[16] *Modern Plastics Handbook*, Technology Seminars, Lutherville, MD, USA, 2000, p. 89.
[17] P. Antunes, F. Domingues, M. Granada, and P. André, "Mechanical properties of optical fibers," in *Selected Topics on Optical Fiber Technology*. London, U.K.: IntechOpen, 2012, pp. 537–550. [Online]. Available: http://www.intechopen.com

ABRAHAM PEREZ-ALONZO received the B.S. degree in electrical and electronic engineering from the Juarez Autonomous University of Tabasco, Tabasco, Mexico, in 2013, and the M.I. degree in electrical engineering from the National Autonomous University of Mexico, Mexico City, Mexico, in 2019, where he is currently pursuing the Ph.D. degree in electrical engineering.

From 2013 to 2016, he was a Field Engineer at E&Tech Developments de Mexico Company, where he was working with electronic instrumentation for oil and gas exploration applications. His research interest includes the design of optical fiber sensors, with a focus on vibration sensors for seismic applications.

FERNANDO VELÁZQUEZ-CARREÓN received the B.Sc. degree in physics, in 2020, and the M.I. degree in electrical engineering from the National Autonomous University of Mexico, Mexico City, in 2022, where he is currently pursuing the Ph.D. degree in electrical engineering.

From 2019 to 2022, he has participated an Associate Collaborator in the ALICE experiment in the European Organization for Nuclear Research, CERN in the design, construction, and instrumentation of a fiber optic scintillator particle detector. His current research interests include the design of scintillator and fiber optics particle detectors and optical fiber sensor for structural health monitoring applications.

GABRIEL EDUARDO SANDOVAL-ROMERO received the master's degree in electrical engineering, in 1995, and the Ph.D. degree in technical sciences from the Saint Petersburg State University of Telecommunications, St. Petersburg, Russia, in 2001. He is currently with the Sensors Group, Institute for Applied Sciences and Technology (ICAT, by its acronym in Spanish), National Autonomous University of Mexico (Universidad Nacional Autónoma de México), Mexico City. He has worked on the development of optical sensors and optical fiber sensors to measure physical magnitudes. His current research interests include fiber optic instrumentation and sensing and monitoring physical, chemical, and biological parameters.